Synthesis of sol-gel synthesized ZnO-CdO nanocomposite for photovoltaic applications

K. P. Sridevi[a], V. Revathi[b], P. Sangeetha[c], B. Manjunatha[d], S. Sivakumar[e, *]

[a]*Department of Physics, Sri Kailash Women's College, Thalaivasal, Tamilnadu, India*
[b]*Department of Physics, New Horizon College of Engineering, Bengaluru, India*
[c]*Department of Physics, Sona College of Technology, Salem, Tamilnadu, India*
[d]*Department of Mechanical Engineering, New Horizon College of Engineering, Bengaluru, India*
[e]*Department of Physics, Government Arts College (Autonomous), Salem, Tamilnadu, India*

Nanocomposites comprising semiconductor materials hold immense potential for advancing photovoltaic technologies due to their unique optoelectronic properties. This research focuses on the synthesis and characterization of a ZnO-CdO (zinc oxide and cadmium oxide) nanocomposite using the sol-gel method for potential application in photovoltaic devices. The sol-gel approach provides a versatile platform for tailoring material properties to enhance photovoltaic performance. The structural, morphological, and optical characteristics of the ZnO-CdO nanocomposite were extensively analyzed using techniques including X-ray diffraction (XRD), scanning electron microscopy (SEM), transmission electron microscopy (TEM), and UV-visible spectroscopy. The XRD analysis confirmed the crystalline nature of the nanoparticles and assessed potential changes in their crystal structure upon nanocomposite formation. SEM and TEM images provided insights into particle size, shape, and distribution, corroborating successful nanocomposite fabrication. This study underscores the significance of sol-gel synthesis in tailoring semiconductor nanocomposites for photovoltaic applications. The characterized structural, optical, and photovoltaic properties provide a foundation for further optimization and integration into advanced photovoltaic devices.

(Received September 23, 2023; February 2, 2024)

Keywords: Nanocomposite, Sol-gel synthesis, ZnO, CdO, Photovoltaic applications, XRD, SEM, TEM

1. Introduction

Nanoparticles of semiconductor materials, such as ZnO and CdO, have been a popular topic of ongoing research worldwide [1-3]. These nanoparticles exhibit size dependent properties, including an energy gap and changes in optical properties, making them highly relevant in technological applications. Zinc oxide (ZnO) is classified as a II-VI semiconductor because according to periodic table, zinc fits to the II group and oxygen belongs to the VI group. It possesses a band gap about 3.37 eV and exhibits excitation binding energy of 60 meV which is high when compared to thermal energy (26 meV). ZnO was one of the first metal oxides to be used as a chemical sensor, and its properties can be modulated by mixing it with CdO, so that it can be used for detecting gases (CO, NO_2, and CH4) [4,5]. By combining various types of semiconductor oxides, it's possible to reduce band gap, which effectively broadens the absorbance spectrum to encompass the visible region of light. This results in the separation of electron-hole pairs when exposed to light, consequently leading to enhanced photo catalytic activity [6]. Amongst an array of elements, the introduction of cadmium (Cd) with ZnO effectively narrow downs the band gap.

* Corresponding author: sivaphotonics@gmail.com
https://doi.org/10.15251/DJNB.2024.191.263

This reduction in band gap arises from the smaller band gap exhibited by CdO in comparison to ZnO.

Low-dimensional structures of ZnO-CdO have demonstrated outstanding gas sensing capabilities [7] as well as heightened conductivity due to their substantial surface-to-volume ratio [8]. In the realm of ZnO-based light emitters and detectors, ZnO-CdO heterojunctions and superlattices play pivotal roles [9]. Numerous research endeavors have been undertaken to delve into the properties and applications of ZnO-CdO nanocomposites. For instance, Ayman et al. [10] crafted ZnO-CdO nanocomposite nanofibers through the electro spinning method and assessed their effectiveness as photocatalysts for wastewater treatment under visible light. Sarvanan et al. [6], on the other hand, synthesized ZnO-CdO nanocomposites via thermal decomposition and examined their photocatalytic prowess in decomposing Methylene blue dye.

These studies collectively illustrate that the integration of CdO with ZnO is highly effective in narrowing the band gap of ZnO and enhancing its photocatalytic properties. In a related study, Meenakshi et al. [11] synthesized ZnO-CdO nanocrystals utilizing the solvothermal method, employing zinc and cadmium acetate, urea and ethyl alcohol as precursors. Notably, the resulting nanocrystals exhibited diverse colors, ranging from pure white (representative of ZnO) to dark yellow (characteristic of CdO), contingent upon the proportion of CdO integrated into the structure. Furthermore, it was observed that the yield of these nanocrystals decreased with an increase in cadmium content within the sample.

Hence, this work focuses on the synthesis of ZnO-CdO nanoparticles using the sol-gel method. The sol-gel method is chosen as it enables the production of well-crystalline and uniformly spherical nanoparticles. The synthesized nanoparticles undergo comprehensive characterization to assess their optical and structural properties. In the synthesis process, a sol-gel solution is prepared by dissolving zinc and cadmium precursors in a suitable solvent. The precursor solution undergoes both hydrolysis and condensation reactions, resulting in the formation of a precursor gel. The gel is subsequently subjected to drying and calcination processes to yield the desired ZnO-CdO nanoparticles.

2. Materials and methods

The synthesis of ZnO-CdO nanocomposites using the sol-gel method involves the following steps: Purchase Analytical Grade Chemicals: Chemicals such as zinc nitrate hexahydrate, cadmium nitrate tetrahydrate, sodium hydroxide, ethanol, and water are obtained in analytical grade and used without further purification. Preparation of Solvent: A mixture of ethanol (50 ml) and water (50 ml) is prepared as the solvent for the synthesis. Sol-Gel Process: In a reaction vessel, 0.5 M zinc nitrate hexahydrate is added as a source of zinc oxide (ZnO), and 0.5 M cadmium nitrate tetrahydrate is added as a source of cadmium oxide (CdO). The mixture is stirred magnetically for 10 minutes at room temperature. Addition of Sodium Hydroxide (NaOH): Sodium hydroxide is incrementally added drop by drop to the reaction mixture, as a precipitating reactant. This initiates the formation of ZnO-CdO nanocomposites. The resulting mixture becomes a thick suspension. Centrifugation: The thick suspensions are subjected to centrifugation at 4500 rpm for 15 minutes. Centrifugation helps in separating the solid precipitates from the liquid supernatant. The supernatant is eliminated through the process of decantation. Washing: The resulting precipitates are rinsed twice with absolute ethanol. After each washing step, the solvent is separated from the solid material through centrifugation. Drying: The collected material is subsequently air-dried overnight to eliminate any residual solvent. This results in the formation of a fine powder. Calcination: The dried powders are subjected to calcination at 500°C. Calcination entails subjecting the material to elevated temperatures to stimulate chemical reactions and further promote the formation of ZnO-CdO nanocomposites. Characterization: The synthesized ZnO-CdO nanocomposites can undergo further characterization using a variety of analytical techniques to assess their structural, morphological, and optical properties. Figure 1 provided below summarizes the key steps involved in the synthesis of ZnO-CdO nanocomposites. It likely illustrates the different stages of the process, such as mixing the precursors, adding NaOH, centrifugation, washing, drying, and calcination.

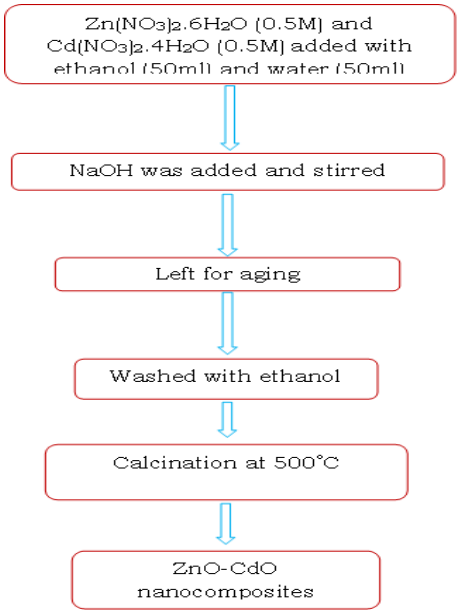

Fig. 1. Processes involved in the fabrication of ZnO-CdO nanocomposites.

3. Characterization method

The ZnO-CdO nanocomposites were characterized using several techniques:

1. XRD: These patterns were obtained using a Mini Flexell- **Desktop** X-ray. CuKα radiation with a wavelength of 1.5406 Å was used. XRD is a technique that provides information about the phase composition of materials and crystal structure and. By analyzing the diffraction pattern, one can determine the crystallographic structure and identify the presence of different phases in the nanocomposites.
2. UV-VIS Spectrophotometry: The optical properties of the nanocomposites were studied using spectrophotometer (named JASCO -V-670). This technique measures the absorption and transmission of light by the materials in the UV and VIS wavelength range. By analyzing the UV-VIS spectrum, information about the bandgap energy, absorbance, and transparency of the nanocomposites can be obtained.
3. Photoluminescence Spectroscopy: These measurements were performed using a Photoluminescence spectrometer named (HORIBA Jobin Yvon) with a 325 nm He-Cd laser. It is a technique that measures the emission of light from a material after it absorbs photonsIt furnishes data regarding the electronic and optical characteristics of the nanocomposites, encompassing aspects like the existence and strength of luminescent emissions.
4. Scanning Electron Microscopy (SEM): The morphologies of the nanocomposites were observed using a JEOL 7001F Field Emission SEM. It provides high resolution imaging of the surface of materials, providing information about their morphology, size, and shape. Furthermore, Energy-Dispersive X-ray Spectroscopy (EDS) was employed alongside SEM to ascertain the composition of the nanocomposites.
5. Transmission Electron Microscopy (TEM): TEM images, along with Selected Area Electron Diffraction (SAED) patterns, were observed using a JEOL JEM 2100 Transmission Electron Microscope. TEM provides high-resolution imaging of the internal structure of materials, allowing for the visualization of individual nanoparticles and their arrangement. SAED patterns provide information about the crystal structure and orientation of the nanocomposites at a higher resolution.

3.1. Structural analysis

This study investigated the structural properties of a ZnO-CdO sample, and its X-ray diffraction pattern shown in figure 2 indicated the presence of wide diffraction peaks corresponding to the hexagonal wurtzite structure of ZnO, along with intensity peaks related to the CdO phase . The robust intensity and slim width of the ZnO-CdO diffraction peaks indicate the high crystalline quality of the resulting products. Two distinct phases were identified in the ZnO-CdO sample: hexagonal ZnO and CdO, with diffraction peaks corresponding to the cubic structure at (1 1 1), (2 0 0), (2 2 0), and (3 1 1), all of which were matched using the JCPDS reference data [ZnO 80-0075 and CdO 05-0640]. In Table 1, it is noteworthy that the characteristic peak (111) associated with the CdO phase shifts from the standard angle of 33.07 to 33.01, indicating a shift toward a lower angle. This phenomenon can be attributed to the substitution of Cd ions by smaller Zn ions within the crystallographic positions. Notably, the ionic radius of $Zn^{(2+)}$ (0.74 Å) is smaller than that of $Cd^{(2+)}$ (0.97 Å). Given their similar electronegativities, Zn ions can readily replace Cd ions in the crystal structure. Consequently, as the volume of the Zn precursor increases, the substitution of Cd ions by smaller Zn ions leads to an increase in the d values and a corresponding decrease in the 2θ angle, causing the peak to shift towards lower angles. Similar findings have been reported in a prior study [12].

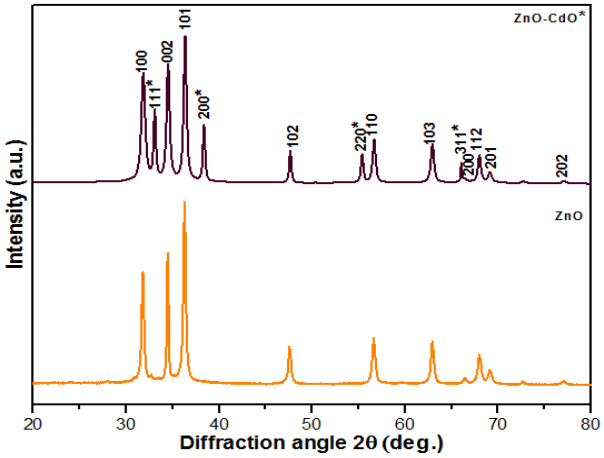

Fig. 2. ZnO-CdO nanocomposites - XRD patterns.

Table 1 displays the crystallite size, which was determined from the XRD data using Scherer's formula.

$$D = \frac{K\lambda}{\beta\ Cos\ \theta}\ (nm)$$

Equations are used to estimate the dislocation density (δ)

$$\delta\ = \frac{15\ \beta\ cos\theta}{4\alpha D}\quad lines\ /\ m^2$$

Using, the micro strain (ε) was computed.

$$\varepsilon = \frac{\beta}{4\tan\theta}$$

Peak positions of different reflection planes exhibit shifts relative to the ideal positions in the presence of stacking faults within the sample. The following equation relates the peak shift in terms of (β) to the chance of stacking faults *(α)*:

$$\alpha = \left[\frac{2\pi^2}{45(3\tan\theta)^{\frac{1}{2}}}\right]\beta\,(\text{Å})$$

where, α - stacking fault

β - Full width at half maximum

Table 1 reveals that the average crystallite size of the ZnO-CdO nanocomposites is 27.66 nm. It is observed that as the crystallite size increases, the dislocation density decreases. Additionally, calculations indicate that both the stacking fault and elastic strains decrease with an increase in crystallite size. X-ray diffraction (XRD) studies confirm that the ZnO-CdO nanocomposites exhibit a good crystalline nature, as evidenced by the high quality of the diffraction patterns. Furthermore, the nanocomposites exhibit lower levels of dislocation, stacking fault, and elastic strains. The reduced values of these parameters indicate that the sol-gel method employed in the synthesis of the ZnO-CdO nanocomposites is an effective technique for producing high-quality polycrystalline materials.

Table 1. Structural parameters of ZnO-CdO nanocomposites.

Planes	**Crystallite Size D (nm)**	**Dislocation Density (δ) (10^{15} lines / m^2)**	**Stacking faults probability (Å)**	**Elastic strains Ɛ**
100	**22.71**	1.9393	0.0058	0.0031
111*	**29.97**	1.1135	0.0043	0.0023
002	**21.49**	2.1660	0.0057	0.0032
101	**25.20**	1.5752	0.0046	0.0027
200*	**30.42**	1.0809	0.0036	0.0022
102	**31.40**	1.0141	0.0029	0.0019
220*	**32.44**	0.9502	0.0024	0.0018

3.2. Photoluminescence spectroscopy

Figure 3 displays the superposition of the photoluminescence (PL) spectra of the ZnO-CdO nanocomposites. Upon observing the PL spectra, two distinct regions can be identified. The first region exhibits a low-intensity peak in the ultraviolet (UV) region at 518 nm, while the second region shows a high-intensity peak in the visible region at 601 nm.

The peak at 518 nm in the UV region corresponds to the near band edge (NBE) emission, which originates from transitions related to excitons. This emission is associated with the energy difference between the valence and conduction band. On the other hand, the peak in the visible region (580-620 nm) represents yellow to orange emissions with higher intensity. This emission is primarily attributed to crystal defects present in the ZnO-CdO nanocomposites, such as Zn interstitials and oxygen vacancies. The orange emission specifically indicates the presence of excess oxygen, while the yellow emission is commonly linked to interstitial oxygen defects (O_i). The yellow emission can also be associated with different initial states, such as the conduction band and shallow donors within the material. It is worth noting that introducing impurities into a semiconductor, as in the case of the ZnO-CdO nanocomposites, can lead to significant changes in its structural and optical properties [13,14]. In this particular case, the introduction of impurities has resulted in the appearance of distinct emission peaks in the PL spectra, corresponding to exciton-related transitions, as well as crystal defects and oxygen-related impurities. References [15,16] likely provide further details and support for the information mentioned in relation to the changes in structural and optical properties induced by impurities in the nanocomposites.

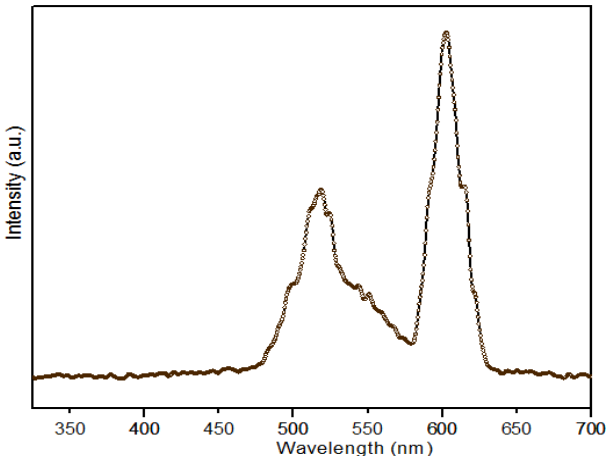

Fig. 3. Photoluminescence spectra of ZnO-CdO nanocomposites

3.3. FT-IR analysis

The FTIR spectrum of ZnO-CdO nanocomposites, depicted in Figure 4, exhibits various absorption bands that provide information about the vibrational modes and chemical bonds present in the material. One prominent feature in the spectrum is the presence of a broad absorption band at approximately 3407 cm−1, which corresponds to the stretching vibrations of hydroxyl (OH) groups in water molecules adsorbed on the surface of ZnO. This observation suggests the presence of water within the ZnO component of the nanocomposite. Another significant band appears at around 1621 cm−1 and can be attributed to the bending vibrations of H_2O molecules, providing further evidence of water content in the nanocomposite. Additionally, stretching vibrations of ZnO and CdO are discerned at approximately 560 cm−1 and 787 cm−1. These bands represent the characteristic vibrational modes of the metal oxides. Additionally, the spectrum may contain other bands corresponding to the bending modes of vibration of metal ion oxygen bonds [17]. These bands are likely observed at different wavenumbers, depending on the specific coordination number and bond length of the metal ions in the nanocomposite. It is important to note that due to the nano size of the grains in the nanocomposite, the IR active modes can experience slight shifts in their wavenumbers. This can be attributed to the differences in coordination number and bond length that arise from the nanoscale structure of the material. However, despite these shifts, the bands around 500 cm^{-1} still exhibit characteristics typical of metal oxides [20-23].

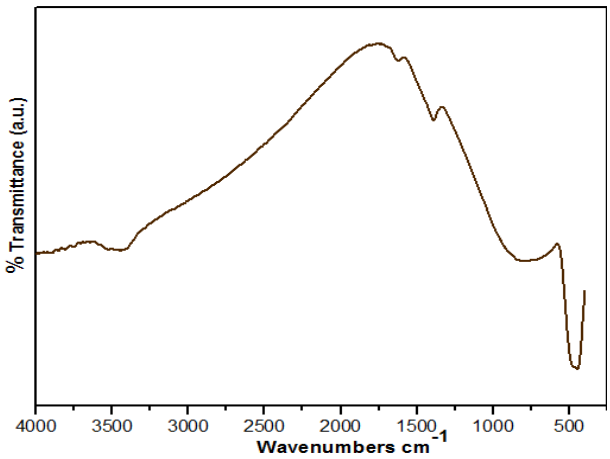

Fig. 4. FTIR spectra of ZnO-CdO nanocomposites

3.4. SEM and EDS analysis

The SEM analysis shown in Figure 5a depicts the ZnO-CdO nanocomposites, which exhibit a spherical shape [18,19]. The spherical shape observed is a consequence of integrating CdO into the ZnO matrix. The SEM images indicate that the sample has a uniform distribution of particles. To analyze the porosity and pore dimensions quantitatively, image processing tools were employed. The processed results show that the particles obtained are homogeneous in shape.

In Figure 5b, the intensity map of the image is displayed following the application of multilevel thresholding with six levels of quantization. Moving to Figure 5c, the darkest portion of the image is singled out and depicted with white pixels set against a uniform black backdrop. Finally, in Figure 5d, the segmented porous spaces within the ZnO samples are presented, with distinct random colors assigned to differentiate between various regions.Finally, the pore size distributions are depicted in Figure 5e, providing information about the range of pore sizes present in the ZnO samples.

Figure 5a displays the original image of the ZnO-CdO nanocomposites, while Figure 5d shows the final processed image after segmentation. The porosity of the nanocomposites is determined to be 0.3924%, with an average pore size of 2.9604 nm and a standard deviation of 2.1425 nm. Comparatively, when using the precursor $Zn(NO_3)_2$ to synthesize ZnO, the porosity was measured to be 0.2431%. The addition of CdO within the ZnO matrix resulted in an increased porosity of 0.3924%. This increase can be attributed to the incorporation of CdO, which affects the crystal structure of ZnO, leading to deformations and a decrease in density. Consequently, the incidence of porosity increases. The higher porosity of the composite also implies higher permeability. The increase in porosity could be due to the replacement of Cd ions with smaller Zn ions in the sample. The synthesized composites with an average pore radius falling within the mesoporous range are suitable for energy storage applications.

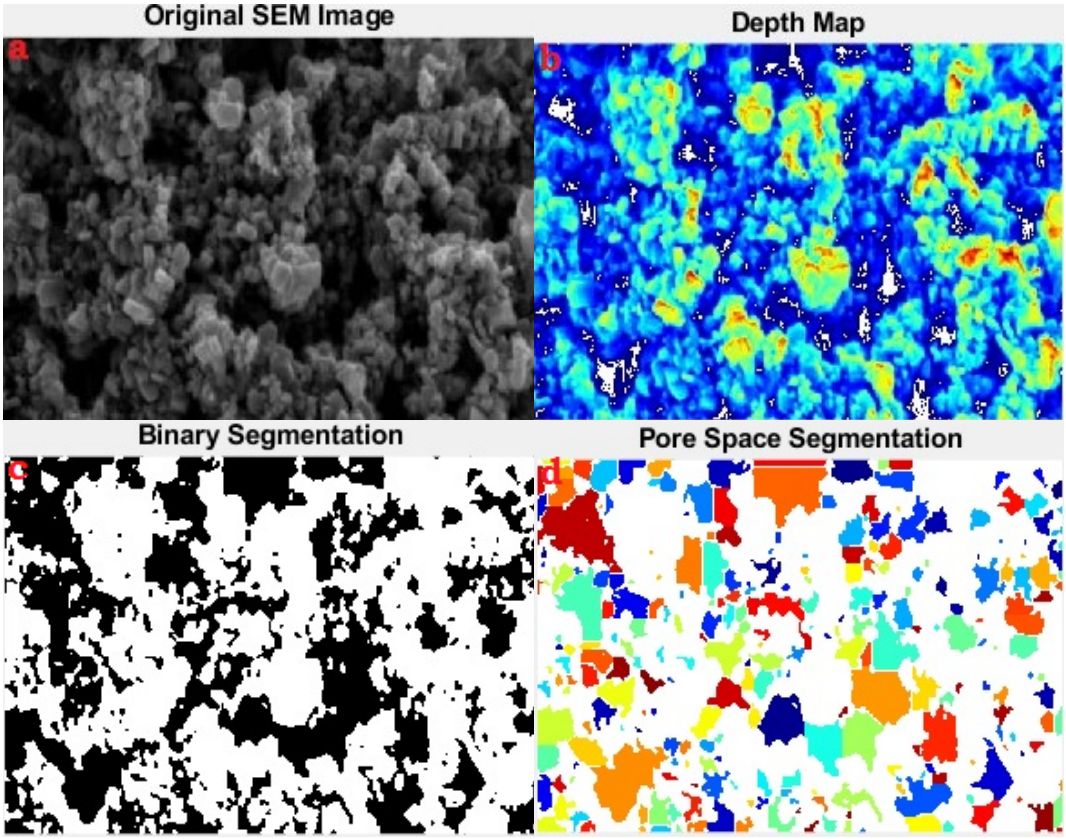

Fig. 5. SEM micrographs of ZnO-CdO nanocomposites

Figure 6 illustrates the 3D surface roughness of the ZnO-CdO nanocomposites, represented by grayscale (a) and color (b) images. These surface roughness features were extracted from SEM images using image processing tools.

Upon comparison with ZnO prepared with zinc nitrate, it is observed that the surface roughness of the ZnO-CdO nanocomposites is increased. This increase in roughness can be attributed to the higher porosity ratio exhibited by the nanocomposites compared to ZnO prepared with zinc nitrate. Therefore, it can be concluded that there is a direct proportionality between surface roughness and porosity.

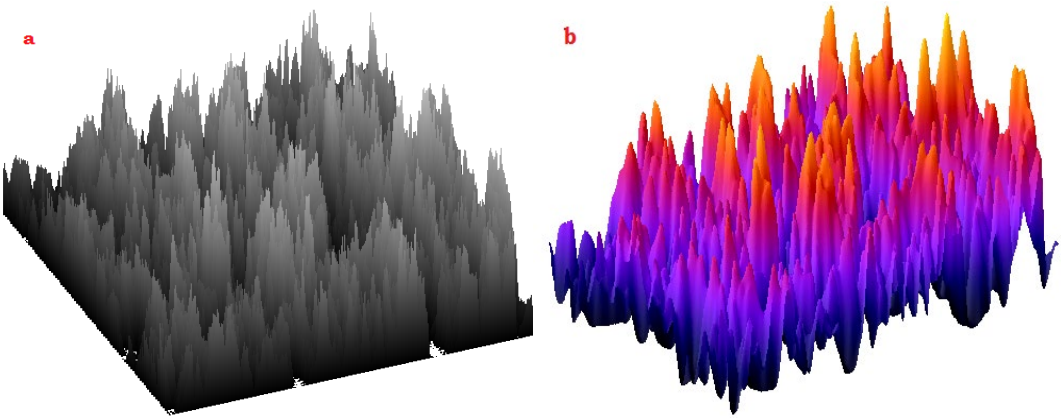

Fig. 6. Surface roughness of ZnO-CdO nanocomposites.

Figure 7 presents the Energy-Dispersive X-ray Spectroscopy (EDS) spectra recorded during the SEM imaging technique. The spectra provide information about the elemental composition of the nanoparticles. In the spectra, peaks around 1.1 keV correspond to the Zn L lines, indicating the presence of zinc in the nanoparticles. Peaks with lower counts observed at 8.7 keV and 9.6 keV are attributed to the Zn Ka and Zn Kb lines, further confirming the presence of zinc. Peaks around 0.5 keV are attributed to the O Ka lines, indicating the presence of oxygen in the nanoparticles. Additionally, peaks observed at 3.15 keV and 3.35 keV correspond to the Cd La and Lb lines, respectively. These peaks indicate the presence of cadmium in the nanoparticles. The inset picture in Figure 7 shows the EDS spectrum of ZnO, providing a reference for the elemental composition. From the EDS spectra, it can be observed that the nanoparticles predominantly contain zinc, oxygen and cadmium.

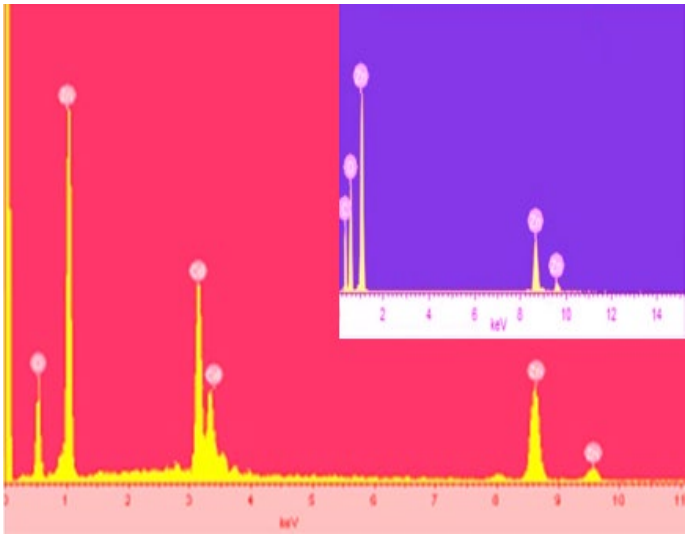

Fig. 7. EDS of ZnO-CdO nanocomposites.

3.5. HRTEM analysis

HRTEM analysis of the ZnO-CdO nanocomposites was performed, and the results are shown in Figure 8a. The nanocomposites exhibited a hexagonal facet and spherical-like morphology with an average size ranging from approximately 21 to 32 nm. This morphology confirmed the presence of a hexagonal wurtzite structure in the nanocomposites. Additionally, small particles were observed to be decorated over the hexagonal facets and spherical structures. To determine the lattice spacing (d-spacing) of the nanocomposites, image processing software tools were employed. Fast Fourier Transform (FFT) and Inverse Fast Fourier Transform (IFFT) of HRTEM images, as shown in Figure 8b. The d-spacing value corresponding to the (100) plane was found to be approximately 0.2815 nm. This value closely matched the corresponding standard values for the hexagonal wurtzite structure, confirming the crystal structure of the nanocomposites. Furthermore, the results obtained from the FFT technique were further processed using Sobel filter tools to detect any defects such as stacking faults and dislocations. The detected defects were then visualized and plotted in Figure 8c. In this plot, the clusters of bluish-green lines denote the positions of defects within the nanocomposite structure.

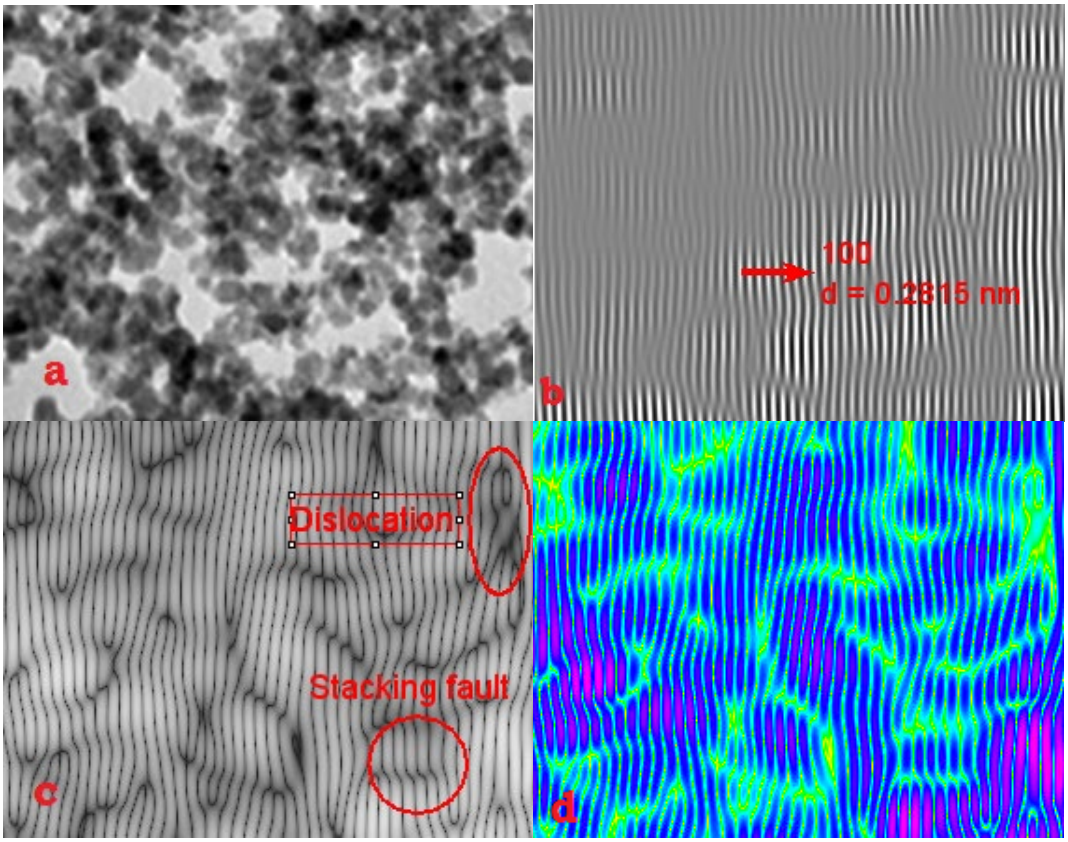

Fig. 8. HRTEM micrographs of ZnO-CdO nanocomposites.

4. Conclusion

ZnO-CdO nanocomposites were prepared via the sol-gel method, employing zinc nitrate hexahydrate and cadmium nitrate tetrahydrate as sources for zinc oxide and cadmium oxide. The synthesis process utilized ethanol and water as solvents. The XRD patterns of the nanocomposites showed wide diffraction peaks corresponding to the hexagonal wurtzite structure of ZnO, as well as intensity peaks indicating the presence of the CdO phase. The intensity and width of the diffraction peaks suggested that the resulting nanocomposites have high crystallinity. The XRD peaks were indexed to the hexagonal ZnO structure and cubic CdO structure using JCPDS reference data (ZnO 80-0075 and CdO 05-0640). The average crystallite size of the

nanocomposites was determined to be 27.66 nm. Additionally, the decrease in dislocation density was observed with an increase in crystallite size. The band gap of the nanocomposites was determined to be 2.4 eV, indicating a band shrinkage effect attributed to the presence of CdO. In the PL spectra, two distinct regions were observed. The peak at 518 nm within the UV region corresponded to near band-edge emission (NBE), associated with exciton-related transitions. Meanwhile, the peak in the visible region spanning 580-620 nm, characterized by its high intensity, represented yellow to orange emission, signifying the existence of crystal defects such as Zn interstitials and oxygen vacancies. The FTIR spectra exhibited stretching vibrations at approximately 560 cm^-1 and 787 cm^-1, corresponding to ZnO and CdO. SEM images revealed that the ZnO-CdO nanocomposites adopted a spherical shape. Quantitative analysis of porosity and pore dimensions was carried out using image processing tools. EDS analysis confirmed the presence of zinc, cadmium, and oxygen elements predominantly within the nanoparticles. TEM images exhibited a spherical morphology, with sizes ranging from approximately 21 to 32 nm. The d-spacing of (100) planes was determined to be 0.2815 nm, and image processing software tools were employed to calculate this d-spacingg and detect defects such as stacking faults and dislocations. The synthesized ZnO-CdO nanocomposites were identified as mesoporous materials, and their pore radius values indicated their suitability for energy storage applications.

References

[1] R. Dash, C. Mahender, P. K.Sahoo, A. Soam, Materials Today: Proceedings, (2020). https://doi.org/10.1016/j.matpr.2020.08.448

[2] S. Shabbir, A. Shaari, B. U. Haq, R. Ahmed, M. Ahmed, Optik, 206, 164285, (2020). https://doi.org/10.1016/j.ijleo.2020.164285

[3] T. Amakali, L. Daniel, V. Uahengo, N. Y. Dzade, N. H. De Leeuw, Crystals, 10(2), 132, (2020) https://doi.org/10.3390/cryst10020132

[4] A. Umar, M. S. Akhtar, M. S. Al-Assiri, A. E. Al-Salami, S. H. Kim, Ceramics International, 44(5), 5017-5024, (2018). https://doi.org/10.1016/j.ceramint.2017.12.098

[5] S. Bai, X. Sun, N. Han, X. Shu, J. Pan, H .Guo, S. Liu, Y. Feng, R. Luo, D. Li, A. Chen, Journal of hazardous materials, 394, 121832, (2020). https://doi.org/10.1016/j.jhazmat.2019.121832

[6] R. Saravanan, H. Shankar, T. Prakash, V. Narayanan, A. Stephen A. Materials Chemistry and Physics, 125(1-2), 277-280, (2011). https://doi.org/10.1016/j.matchemphys.2010.09.030

[7] N. Varghese, L. S. Panchakarla, M. Hanapi, A. Govindaraj, C. N. R. Rao, Materials Research Bulletin, 42(12), 2117-2124, (2007). https://doi.org/10.1016/j.materresbull.2007.01.017

[8] Z. Bi-Ju, L. Jian-She, Z. Lei, J. Qing, Chinese Physics Letters, 28(1), 016801, (2011). 10.1088/0256-307X/28/1/016801

[9] D. J. Winarski, Doctoral dissertation, Bowling Green State University, (2019).

[10] Yousef, A Ayman, N. A. Barakat, T. Amna, A. R. Unnithan, S. S. Al-Deyab, H. Y. Kim, Journal of Luminescence, 132(7), 1668-1677, (2012),. https://doi.org/10.1016/j.jlumin.2012.02.031

[11] Sundar S. Meenakshi, C. K. Mahadevan, P. Ramanathan, Materials and manufacturing processes, 22(3), 400-403, (2007). https://doi.org/10.1080/10426910701190998

[12] L. T. Jule, F. B. Dejene, A. G. Ali, K. T. Roro, A. Hegazy, N. K. Allam, E. El Shenawy, Journal of Alloys and Compounds, 687, 920-926,(2016). https://doi.org/10.1016/j.jallcom.2016.06.176

[13] E. Mosquera, I. del Pozo, M. Morel, Journal of Solid State Chemistry, 206, 265-271, (2013) . https://doi.org/10.1016/j.jssc.2013.08.025

[14] R. Chandiramouli, B. G. Jeyaprakash, Solid State Sciences, 16,102-110, (2013). https://doi.org/10.1016/j.solidstatesciences.2012.10.017

[15] S. Benzitouni, M. Zaabat, M. S. Aida, J. Ebothe, J. Michel, B. Boudine, L. Mansouri, T.

Saidani, Optik, 156, 949-960, (2018). https://doi.org/10.1016/j.ijleo.2017.12.039

[16] R. Saravanan, F .Gracia, M. M. Khan, V. Poornima, V. K.Gupta, V. Narayanan, A. Stephen, Journal of molecular liquids, 209, 374-380, (2015). https://doi.org/10.1016/j.molliq.2015.05.040

[17] N. Rana, S. Chand, A. K. Gathania, Ceramics International, 41(9), 12032-12037,(2015). https://doi.org/10.1016/j.ceramint.2015.06.017

[18] X. Cai, D. Hu, S. Deng, B. Han, Y. Wang, J. Wu, Y. Wang, Sensors and Actuators B: Chemical, 198, 402-410,(2014). https://doi.org/10.1016/j.snb.2014.03.093

[19] T. K. Pathak, J. K. Rajput, V. Kumar, L. P. Purohit, H. C. Swart, R. E. Kroon, Journal of Colloid and Interface Science, 487, 378-387,(2017) https://doi.org/10.1016/j.jcis.2016.10.062

[20] Sridevi, K.P., Prasad, L.G., Sangeetha, B. and Sivakumar, S., Journal of Ovonic Research, 18(3), 453-464,(2022). https://doi.org/10.15251/JOR.2022.183.453

[21] Jasima, F.H., Shakirb, H.R., Chiada, S.S., Habubic, N.F., Mosad, Z.S.A., Kadhime, Y.H. and Jadanf, M., Digest Journal of Nanomaterials & Biostructures, 18(4), (2023). https://doi.org/10.15251/DJNB.2023.184.1385

[22] Santhosh, M., Satheeskumar, S., Shanthi, C. and Bhuvaneswari, B.V., Journal of Ovonic Research, 18(2), (2022). https://doi.org/10.15251/JOR.2022.182.113

[23] Santhi, R., Shanthi, C., Sathya, M. and Pushpanathan, K., J. Chem. Pharm. Res., 8(9), 249-259, (2016).